

1           **When does vapor pressure deficit drive or reduce**  
2           **evapotranspiration?**

3           **A. Massmann<sup>1</sup>, P. Gentine<sup>1</sup>, C. Lin<sup>2</sup>**

4           <sup>1</sup>Department of Earth and Environmental Engineering, Columbia University, New York, NY 10027

5           <sup>2</sup>Department of Hydraulic Engineering, Tsinghua University, Beijing, CN

6           **Key Points:**

- 7           • = enter point 1 here =  
8           • = enter point 2 here =  
9           • = enter point 3 here =

10      **Abstract**

11      = enter abstract here =

12      **1 Introduction**

13      Changes to vapor pressure deficit (VPD) alter the atmospheric demand for water from  
 14      the land surface. Traditionally, atmospheric scientists and hydrometeorologists generally  
 15      think that an increase in atmospheric demand induces an increases in evapotranspiration  
 16      (ET) (citations?). This possible misconception developed in part due to the proliferation of  
 17      studies examining potential ET rather than estimates of ET itself (citations?). In contrast, plant  
 18      physiologists know that stomata have evolved to optimally regulate the exchange of water  
 19      and carbon, and tend to close in response to increased atmospheric dryness [??*MEDLYN*  
 20      *et al.*, 2011]. Therefore, an increase (decrease) in VPD may not correspond to an increase  
 21      (decrease) in ET because stomatal closure (opening) can cancel the effects of shifts to atmo-  
 22      spheric demand.

← This section  
needs to be  
fleshed out,  
and I defi-  
nitely need  
to add more  
citations

23      Quantifying the plant response to a perturbation to atmospheric VPD increases our un-  
 24      derstanding of land surface response to shifts in atmospheric conditions. If plant response  
 25      reduces ET in response to atmospheric drying then soil moisture will be conserved. An in-  
 26      crease in ET in reponse to atmospheric drying will reduce soil moisture, but contribute in-  
 27      creased moisenting to the atmosperhere. Clearly, the sign and magnitude of land-surface  
 28      responsedrives the co-evolution of the atmosphere and land-surface at many timescales, from  
 29      diurna to interdecadal.

30      In order to quantify plant response to perturbations to atmospheric demand for water,  
 31      we apply a Penman-Monteith framework to eddy-covariance observation spanning various  
 32      biomes and climates. Section 2 describes the data used, Section 3 derives the framework,  
 33      Section 4 presents results, and Section 5 discusses conclusions. The goal of this paper is  
 34      to use reasonable approximations as a tool to increase intuition for plant response to atmo-  
 35      spheric drying. This intuition will aid interpretation of observations and full complexity cli-  
 36      mate models.

37      **2 Methods**

38      The Penman-Monteith equation (hereafter PM) estimates ET as a function of atmo-  
 39      spheric and land-surface variables:

$$40 \quad ET = \frac{\Delta R + g_a \rho_a c_p D_s}{\Delta + \gamma(1 + \frac{g_a}{g_s})}, \quad (1)$$

41 where variable definitions are given in Table 1. *MEDLYN et al.* [2011] developed a  
 42 model for  $g_s$  by combining optimal photosynthesis theory with empirical approaches. The  
 43 result for leaf-scale stomatal resistance was:

$$44 \quad g_{l-s} = g_0 + 1.6 \left(1 + \frac{g_1}{\sqrt{D_s}}\right) \frac{A}{c_s} \quad (2)$$

45 This can be adapted to an ecosystem-scale stomatal resistance by multiplying by leaf  
 46 area index (LAI) and converting units to  $\text{m s}^{-1}$ :

$$47 \quad g_s = \text{LAI} \frac{RT}{P} \left(g_0 + 1.6 \left(1 + \frac{g_1}{\sqrt{D_s}}\right) \frac{A}{c_s}\right) \quad (3)$$

48 While Equation 3 can be used in PM, it will make analytical work with the function  
 49 intractable because  $A$  is a function of ET itself. To remove dependence of ET on  $A$  we can  
 50 use the semi-empirical results of *Zhou et al.* [2015]. *Zhou et al.* [2015] showed that:

$$51 \quad uWUE = \frac{GPP \cdot \sqrt{D}}{ET} \quad (4)$$

52 is relatively constant across time and space (within plant functional type). If, following *Lin*  
 53 *et al.* [2015], we approximate  $g_0$  as 0, we can use  $uWUE$  to remove  $A$  from  $g_s$  in a way that  
 54 makes PM analytically tractable:

$$55 \quad g_s = \frac{\text{LAI}}{\text{LAI}_{ref}} \frac{RT}{P} 1.6 \left(1 + \frac{g_1}{\sqrt{D_s}}\right) \frac{uWUE \cdot ET}{c_s \sqrt{D}} \quad (5)$$

56 Note that  $uWUE$  is fit on the ecosystem scale in *Zhou et al.* [2015] so it already has an  
 57 implicit  $\text{LAI}_{ref}$  reflective of the average  $LAI$  in *Zhou et al.* [2015]'s fits. So the LAI term  
 58 in Equation 2 becomes a term we call  $\frac{\text{LAI}}{\text{LAI}_{ref}}$ , which is a measure of how close the observed  
 59 LAI is to the  $\text{LAI}_{ref}$  in *Zhou et al.* [2015].

60 Next, plugging Equation 5 into Equation 1 and rearranging gives:

$$61 \quad ET = \frac{\Delta R + \frac{g_a P}{T} \left(\frac{c_p D_s}{R_{air}} - \frac{\text{LAI}_{ref}}{\text{LAI}} \frac{\gamma c_s \sqrt{D}}{R * 1.6 uWUE (1 + \frac{g_1}{\sqrt{D}})}\right)}{\Delta + \gamma} \quad (6)$$

62 We can then take the derivative with respect to  $D$  to analytically determine ecosystem  
 63 response to atmospheric demand perturbations:

$$64 \quad \frac{\partial ET}{\partial D} = \frac{g_a P}{T(\Delta + \gamma)} \left( \frac{c_p}{R_{air}} - \frac{\text{LAI}_{ref}}{\text{LAI}} \frac{\gamma c_s}{1.6 R * \text{uWUE}} \left( \frac{2g_1 + \sqrt{D}}{2(g_1 + \sqrt{D})^2} \right) \right) \quad (7)$$

65 Note that given yearly uWUE from Zhou et al. [2015],  $g_1$  from Lin et al. [2015] [as presented  
 66 in Franks et al., 2017], and observations of R, T, P,  $D_s$ , and wind speed (WS), the only un-  
 67 known is  $\frac{\text{LAI}}{\text{LAI}_{ref}}$ . With flux tower observations of ET,  $\frac{\text{LAI}}{\text{LAI}_{ref}}$  will then be uniquely deter-  
 68 mined for each observation through Equation 6:

$$69 \quad \frac{\text{LAI}}{\text{LAI}_{ref}} = - \frac{g_a \gamma c_s \sqrt{D_s} P}{(\text{ET} (\Delta + \gamma) - \Delta R - g_a \rho_a c_p D_s) 1.6 R T \text{ uWUE} (1 + \frac{g_1}{\sqrt{D_s}})} \quad (8)$$

70 This  $\frac{\text{LAI}}{\text{LAI}_{ref}}$  is some part a “true” deviation of LAI from  $\text{LAI}_{ref}$  in Zhou et al. [2015],  
 71 and some part model and observational error, including assumptions about constant  $g_1$  and  
 72  $uWUE$ . By calculating a unique  $\frac{\text{LAI}}{\text{LAI}_{ref}}$  for each observation we will propagate any model  
 73 and observational uncertainty forward into our expression for  $\frac{\partial ET}{\partial D}$ .

### 75 3 Data

76 We use data from FLUXNET2015. Because  $g_1$  coefficients [Lin et al., 2015] and uWUE  
 77 were only both available for five plant functional types (PFTs - see Table 2), only 56 of the 77  
 78 sites were used. Figure 1 presents each site and its plant functional type.

84 We restrict our analysis to the daytime (sensible heat  $> 5 \text{ W m}^{-2}$  and shortwave radia-  
 85 tion  $> 50 \text{ W m}^{-2}$ ) when there is no precipitation and the plants are growing (GPP  $> 10\%$  of  
 86 the 95th percentile). Also, because some sites use half hourly data but some use hourly, we  
 87 aggregate all data to hourly averages. Only times with good quality control flags are used.

← map needs  
to be im-  
proved - it's  
a placeholder  
for now

### 88 4 Results

89 By construction, the variability in the  $\frac{\text{LAI}}{\text{LAI}_{ref}}$  term (Equation 8) contains all model  
 90 and observational uncertainties. We expect LAI to be close to  $\text{LAI}_{ref}$ , so  $\frac{\text{LAI}}{\text{LAI}_{ref}}$  should be  
 91  $O(1)$ . We can have some confidence in our framework, including the assumption of constant  
 92 uWUE, if calculated  $\frac{\text{LAI}}{\text{LAI}_{ref}}$ s are generally  $O(1)$ . Figure 2 presents the histogram of calcu-  
 93 lated  $\frac{\text{LAI}}{\text{LAI}_{ref}}$ s with outliers (lowest and highest 5% percent) and nonphysical values ( $\frac{\text{LAI}}{\text{LAI}_{ref}}$

← This GPP  
thresholding  
was used by  
Changjie, do  
you know if  
there is a ci-  
tation for it?  
Otherwise it  
seems like  
something  
a reviewer  
would have  
issue with as  
it is arbitray

74

**Table 1.** Definition of symbols and variables

Variable	Description	Units
$e_s$	saturation vapor pressure	Pa
$T$	temperature	K
$\Delta$	$\frac{\partial e_s}{\partial T}$	Pa K <sup>-1</sup>
$R$	net radiation at land surface minus ground heat flux	W m <sup>-2</sup>
$g_a$	atmospheric conductance	m s <sup>-1</sup>
$\rho_a$	air density	kg m <sup>-3</sup>
$c_p$	specific heat capacity of air at constant pressure	J K <sup>-1</sup> kg <sup>-1</sup>
$D$	VPD	Pa
$\gamma$	psychrometric constant	Pa K <sup>-1</sup>
$g_s$	stomatal conductance	m s <sup>-1</sup>
$g_{l-s}$	leaf-scale stomatal conductance	mol m <sup>-2</sup> s <sup>-1</sup>
$R^*$	universal gas constant	J mol <sup>-1</sup> K <sup>-1</sup>
$LAI$	leaf area index	-
$\frac{LAI}{LAI_{ref}}$	ratio of LAI to LAI <sub>ref</sub> in Zhou <i>et al.</i> [2015]	-
$c_s$	CO <sub>2</sub> concentration	$\mu$ mol CO <sub>2</sub> mol <sup>-1</sup> air

<sup>a</sup>Footnote text here.

79

80

81

**Table 2.** Plant functional types, their abbreviation, Medlyn coefficient [from Lin *et al.*, 2015], and uWfUE [from Zhou *et al.*, 2015]. Note that units are converted such that the quantities fit into Equations 1-8 with the variables in Table 1.

Abbreviation	PFT	$g_1$ (Pa <sup>0.5</sup> )	uWUE ( $\mu$ -mol [C] Pa <sup>0.5</sup> J <sup>-1</sup> [ET])
CRO	cropland	183.1	3.80
CSH	closed shrub	148.6	2.18
DBF	deciduous broadleaf forest	140.7	3.12
ENF	evergreen needleleaf forest	74.3	3.30
GRA	grassland (C3)	166.0	2.68

<sup>a</sup>Footnote text here.

94 < 0.) removed. All remaining  $\frac{\text{LAI}}{\text{LAI}_{ref}}$  values are  $O(1)$  which provides confidence in model  
95 framework.

99 An additional concern is that the  $\frac{\text{LAI}}{\text{LAI}_{ref}}$  term may in fact be some function of  $D$ , in  
100 which case the dependence would need to be accounted for when taking the derivative. Fig-  
101 ure 3. plots the joint distribution of  $\frac{\text{LAI}}{\text{LAI}_{ref}}$  and VPD, and shows that  $\frac{\text{LAI}}{\text{LAI}_{ref}}$  is very weakly a  
102 function of VPD. Given this weak dependence, we argue that Equation 7 is a valid approxi-  
103 mation for ET response to  $D$ .

108 Before calculating the sensitivity of ET to VPDn, it is useful to consider the functional  
109 form of Equation 7. There are three terms: a scaling term for the full expression we will call  
110 Term 1 ( $\frac{g_a P}{T(\Delta+\gamma)}$ ), a relatively constant offset we will call Term 2 ( $\frac{c_p}{R_{air}}$ ), and a variable term  
111 we will call Term 3 ( $\frac{\text{LAI}_{ref}}{\text{LAI}} \frac{\gamma c_s}{1.6 R \text{ uWUE}} \left( \frac{2g_1 + \sqrt{D}}{2(g_1 + \sqrt{D})^2} \right)$ ). All variables are positive, so the relative  
112 magnitude between Term 2 and Term 3 will determine the sign of the derivative, while Term  
113 1 will scale the expression larger or smaller.

114 In Term 1,  $\frac{P}{T} \propto \rho$ , so this should vary little relative to  $g_a$  and  $\Delta$ .  $\gamma$  should also be rel-  
115 atively constant. So the scaling term, Term 1, should be primarily a function of  $g_a$  and tem-  
116 perature (through the function  $\Delta$ ). While temperature range may vary for PFT, the functional  
117 form of  $\Delta$  will be the same.  $g_a$  will vary strongly with PFT due to the importance of surface  
118 roughness. However, the coefficient of variability for both  $g_a$  and Term 1 is relatively con-  
119 stant across PFT, suggesting that the influence of  $g_a$  on the relative (to the mean) variability  
120 of Term 1 is approximately similar across PFT.

121 Figure 4A shows Term 1 normalized by mean  $g_a$  (calculated for each plant functional  
122 type), and confirms that much of the relative variability of Term 1 is contained in the  $g_a$   
123 term's relative variability. Generally,  $T$  has less of a role. Additionally, the impact of  $T$  on  
124 the relative variability increases with increasing  $g_a$ .

125 While the relative variability of Term 1 is similar across PFT, the absolute value of  
126 Term 1 varies strongly across PFT. Figure 4B shows Term 1 evaluated with the mean  $g_a$  for  
127 each PFT, and at the range of observed temperatures for each PFT. As expected, for the tree  
128 PFTs (DBF, ENF) Term 1 is much larger and the temperature dependence is much stronger.  
129 Systematic differences in observed temperatures also cause differences in the average mag-  
130 nitude of Term 1. For example, ENF experiences on average colder temperatures and is thus  
131 more likely to have a larger scaling term. Additionally, because  $\text{std}(g_a) \propto \overline{g_a}$ , the spread of

← Figs 2 and 3  
can probably  
be combined  
- the his-  
togram of  
 $\frac{\text{LAI}}{\text{LAI}_{ref}}$  is  
shown in Fig  
3

132 Term 1 due to  $g_a$  variability will be larger for the tree PFTs, although this is not shown for  
 133 simplicity. To summarize, the variability of Term 1 within each PFT will look like Figure 4A  
 134 for each PFT, but the scale of the x and y-axis will increase or decrease according to mean  $g_a$   
 135 observed in Figure 4B.

140 Term 2 minus Term 3 determines the sign of the sensitivity of ET to VPD and is thus  
 141 crucial.  $c_s$  variability is relatively less than  $\frac{\text{LAI}}{\text{LAI}_{ref}}$  and  $D$  variability, then variability within  
 142 PFT will be solely determined by  $\frac{\text{LAI}}{\text{LAI}_{ref}}$  and  $D$  at the different fluxnet sites. Figure 5 shows  
 143 how (Term 2 - Term 3) varies with  $D$  and  $\frac{\text{LAI}}{\text{LAI}_{ref}}$ , as a function of PFT. In Figure 5a lower  
 144 uWUE and  $\frac{\text{LAI}}{\text{LAI}_{ref}}$  shift the distribution of (Term 2 - Term 3) towards negative values. Addi-  
 145 tionally, the smaller  $g_1$ , the greater the relative  $D$  dependence of (Term 2 - Term 3). This  
 146 is observed most strongly for the ENF PFT, which has the smallest  $g_1$  (74.31).

153 Figure 5b shows the location of the minima of ET, as a function of  $\frac{\text{LAI}}{\text{LAI}_{ref}}$  and  $D$ . For  
 154 any  $\frac{\text{LAI}}{\text{LAI}_{ref}}$  or VPD less (more) than these curves, Term 2 - Term 3 will be negative (positive).  
 155 It is clear that the portion of VPD observations below/above these curves will be a strong  
 156 function of  $\frac{\text{LAI}}{\text{LAI}_{ref}}$ . However, we can see some general trends. For CSH,  $\frac{\partial ET}{\partial D}$  should be neg-  
 157 ative for the vast majority of observed  $\frac{\text{LAI}}{\text{LAI}_{ref}}$  and VPD. The fraction of positive  $\frac{\partial ET}{\partial D}$  appears  
 158 to be more even for ENF, GRA, and DBF, and we might expect a greater frequency of posi-  
 159 tive  $\frac{\partial ET}{\partial D}$  for CRO.

160 Table 3 confirms these expectations for PFT behavior of  $\frac{\partial ET}{\partial D}$ . For all PFTs except for  
 161 CRO, average  $\frac{\partial ET}{\partial D}$  is less than zero. However,  $\frac{\partial ET}{\partial D}$  evaluated at the average of all variables  
 162 (e.g.  $\frac{\text{LAI}}{\text{LAI}_{ref}}$ ,  $T$ ,  $c_s$ ,  $D$ ) is only negative for CSH and GRA. And, DBF in addition to CRO  
 163 experiences  $\frac{\partial ET}{\partial D} < 0$  less than half the time. These observations highlight the effect of the  
 164 nonlinear function in Figure 5:  $\frac{\partial ET}{\partial D}$  has a much steeper slope when the function is negative,  
 165 and is thus more likely to be large.

166 The units of  $\frac{\partial ET}{\partial D}$  make it difficult to interpret if  $D$  is even a meaningful contributor to  
 167 ET's variability. To better understand  $D$ 's contribution, we normalize  $\frac{\partial ET}{\partial D}$  with  $D$ 's standard  
 168 deviation to define a (linearized) relative change in ET for variations in  $D$ .  $D$ 's contribu-  
 169 tion to ET's variability ranges between 16 - 20 W m<sup>-2</sup> for all PFTs except for CSH, which  
 170 is about 51 W m<sup>-2</sup>. Another meaningful comparison is to  $\frac{\partial ET}{\partial R} * std(R)$ , as net radiation is  
 171 generally the driver of ET (cite joe berry here). For all PFTs except for CSH  $D$  contributes  
 172 between 14.5 - 20.5 % of  $R$ 's contribution to variability. For CSH the portion is much larger,  
 173 about 44 %.  $D$ 's variability is certainly a non-negligible contributor to ET's variability.

187

**Table 3.** Statistics of  $\frac{\partial ET}{\partial D}$  as a function of PFT.

PFT	$\overline{\frac{\partial ET}{\partial VPD}}$	$\overline{\frac{\partial ET}{\partial D}}(\overline{T}, \dots, \overline{D})$	$\overline{\frac{\partial ET}{\partial D}}(\overline{T}, \dots, \overline{D}) * \text{std}(D)$	$\frac{\overline{\frac{\partial ET}{\partial D}}(\overline{T}, \dots, \overline{D}) * \text{std}(D)}{\overline{\frac{\partial ET}{\partial R}}(\overline{T}, \dots, \overline{D}) * \text{std}(R)}$	fraction $\frac{\partial ET}{\partial VPD} < 0$
CRO	0.000853	0.026241	18.523659	0.203022	0.473311
CSH	-0.108234	-0.091526	50.861613	0.439379	0.931660
DBF	-0.012727	0.013794	19.734435	0.164241	0.461674
ENF	-0.034087	0.000706	16.611852	0.148548	0.534425
GRA	-0.019637	-0.000921	16.798083	0.173552	0.631735

<sup>a</sup>Footnote text here.

174 So far, idealized plots and statistics have illuminated the form of  $\frac{\partial ET}{\partial D}$  and how it varies  
 175 with PFT. Large mean  $\frac{\text{LAI}}{\text{LAI}_{ref}}$  and uWUE shifts CRO and DBF towards positive  $\frac{\partial ET}{\partial D}$ . How-  
 176 ever, the strongly nonlinear function of  $\frac{\partial ET}{\partial D}$  at  $\frac{\partial ET}{\partial D} < 0$  pushes  $\overline{\frac{\partial ET}{\partial D}}$  negative for DBF (it  
 177 does not do this for CRO because of CRO's high  $g_1$ ). ENF's low  $g_1$  value increases the de-  
 178 pendence of  $\frac{\partial ET}{\partial D}$  on  $D$ , and makes the function more strongly nonlinear. This has the side  
 179 effect of pushing  $\overline{\frac{\partial ET}{\partial D}}$  negative further than other PFTs for a given fraction  $\frac{\partial ET}{\partial D} < 0$  and  
 180 magnitude  $\overline{\frac{\partial ET}{\partial D}}(\overline{T}, \dots, \overline{D})$ . GRA shows the opposite behavior; a relatively high  $g_1$  makes  
 181 the function more linear, decreasing the magnitude of  $-\overline{\frac{\partial ET}{\partial D}}$  for a given [large] fraction  
 182  $\frac{\partial ET}{\partial D} < 0$  and negative  $\overline{\frac{\partial ET}{\partial D}}(\overline{T}, \dots, \overline{D})$  (although  $g_a$  and Term 1 also probably have a role in  
 183 this). Finally, low uWUE of CSH pushes toward by far the lowest values  $\frac{\partial ET}{\partial D}$  (Figure 5).  
 184 Variability in  $D$  accounts for the largest about of  $ET$  variability for CSH. For the other PFTs,  
 185  $D$  contributes less to  $ET$  variability, but still represents about 15-20 % of  $R$ 's contributions  
 186 to  $ET$  variability.

#### 188 4.1 Full observations of $\frac{\partial ET}{\partial D}$

189 Now that we have an intuitive understanding of  $\frac{\partial ET}{\partial D}$ 's behavior, we are equipped to  
 190 interpret fully realistic plots of  $\frac{\partial ET}{\partial D}$  for each PFT. Figure 6 presents calculated  $\frac{\partial ET}{\partial D}$  where,  
 191 unless otherwise noted, all variables in Equation 7 are allowed to vary. Each column is a  
 192 different quantity related to  $\frac{\partial ET}{\partial D}$ , and each row is a different PFT.

193 The full observations generally confirm expectations from Section 4. CRO has the  
 194 most positive values of  $\frac{\partial ET}{\partial D}$ ,  $\frac{\partial ET}{\partial D}$  is almost always negative for CSH, and response depends  
 195 more with the environmental conditions for the other PFTs (especially ENF). Through the

columns of Figure 6 we can see the impact of  $\frac{\text{LAI}}{\text{LAI}_{ref}}$  and  $g_a$  on the variability of  $\frac{\partial ET}{\partial D}$ .  $g_a$ 's scaling (included in columns 1 and 3) alters the magnitude considerably.  $\frac{\text{LAI}}{\text{LAI}_{ref}}$  variability (included in columns 1 and 2) adds a lot of additional noise to the signal of  $\frac{\partial ET}{\partial D}$ , which is slightly undesirable given  $\frac{\text{LAI}}{\text{LAI}_{ref}}$ 's role in representing model and observational uncertainty. However, the general story with the noise appears to match the cleaner signal when  $\frac{\text{LAI}}{\text{LAI}_{ref}}$  is held constant and  $D_{ETmin}$  is clearly visible. One exception is possibly with GRA, for which uncertainty represented in  $\frac{\text{LAI}}{\text{LAI}_{ref}}$  is high and causes the full complexity plots (Columns 1 and 2) to not match well with  $\frac{\text{LAI}}{\text{LAI}_{ref}}$  held fixed (Columns 3 and 4).

← I really need to make these plots better - way too much overlapping of points that hurts the story

For ENF and GRA  $D_{ETmin}$  does not appear to be only a function of  $\frac{\text{LAI}}{\text{LAI}_{ref}}$  (most observable in Column 4). It turns out that the site to site variability in  $\gamma$  causes  $D_{ETmin}$  to vary, which is not discussed in the previous section. The impact is observable in both ENF and GRA, but especially for ENF which has a larger  $\frac{\partial^2 ET}{\partial^2 D}$  than the other PFTs.

In general the full complexity plots of  $\frac{\partial ET}{\partial D}$  match our expectations, even with the large sensitivity to  $\frac{\text{LAI}}{\text{LAI}_{ref}}$  measures of uncertainty observed in Figure 5. Our  $\frac{\text{LAI}}{\text{LAI}_{ref}}$ -based method of uncertainty propagation blurs the idealized expectations the most for GRA, and also has a considerable effect for CRO. We therefor have the most confidence in our conclusion based on Equation 7 for PFTS CSH, DBF, and ENF, as the full complexity plots with uncertainty included closely match the story when  $\frac{\text{LAI}}{\text{LAI}_{ref}}$  is held fixed. \*\*see somewhat preferred alternate figure 7 .

← I think I like the alternate plot much more as thinking in terms of T and RH is easier, and it makes the story easier to see at relatively low temperatures. However, I used the other plot because Fig 5 does not discuss things in terms of temperature, as this would make things more complicated (adding another dimension).

## 5 Conclusions

The idealized representation of ET used here is successful in developing intuition for how ET responds to changes in  $D$ . This intuition will aid the community in interpreting observations and output from sophisticated full complexity climate models.

The idealized framework leads to the following general conclusions:

- Aerodynamic resistance plays an important role of scaling  $\frac{\partial ET}{\partial D}$ . This is a leading order effect for observing higher magnitude responses in DBF and ENF.
- In general, CSH has the most negative (i.e. ET reduced) response to increases in  $D$  (atmospheric drying). So CSH plants will almost always try and conserve water, effectively reducing ET with dry atmospheric perturbation.
- Additionally for CSH,  $D$  variability contributes the most to  $ET$  variability.

- CRO has the most positive response (i.e. ET increased) in response to increases in  
D. This is consistent with CROs that may be evolved or bred to thrive in non-water-limited environments.
- The response is more a function of the environment for DBF, ENF, and GRA. Because as VPD increases the response is more likely to be positive, if RH is fixed then the response will be more likely to be positive at warmer T, or if T is fixed the response is more likely to be positive with decreasing RH.
- ENF has the strongest dependence on environmental conditions due to its small  $g_1$ .
- Model and observational uncertainty is highest for GRA and CRO, so conclusions about those PFTs should be tempered.
- However, inclusion of uncertainty doesn't alter conclusions about DBF, ENF, and CSH.

The intuition developed using this framework can be used to understand how the land surface will respond and contribute to changes in the environment.

## Acknowledgments

This work used eddy covariance data acquired and shared by the FLUXNET community, including these networks: AmeriFlux, AfriFlux, AsiaFlux, CarboAfrica, CarboEuropeIP, CarboItaly, CarboMont, ChinaFlux, Fluxnet-Canada, GreenGrass, ICOS, KoFlux, LBA, NECC, OzFlux-TERN, TCOS-Siberia, and USCCC. The ERA-Interim reanalysis data are provided by ECMWF and processed by LSCE. The FLUXNET eddy covariance data processing and harmonization was carried out by the European Fluxes Database Cluster, AmeriFlux Management Project, and Fluxdata project of FLUXNET, with the support of CDIAC and ICOS Ecosystem Thematic Center, and the OzFlux, ChinaFlux and AsiaFlux offices.

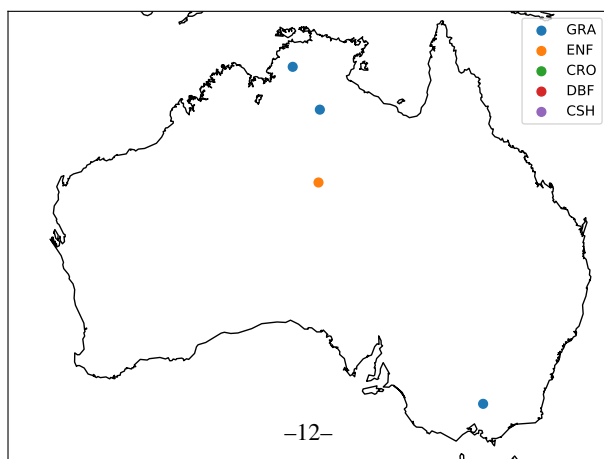
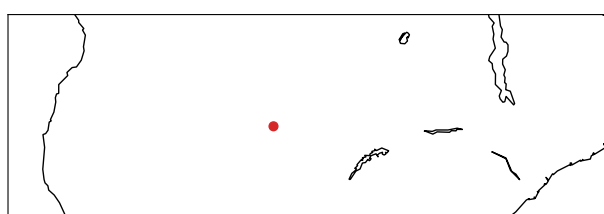
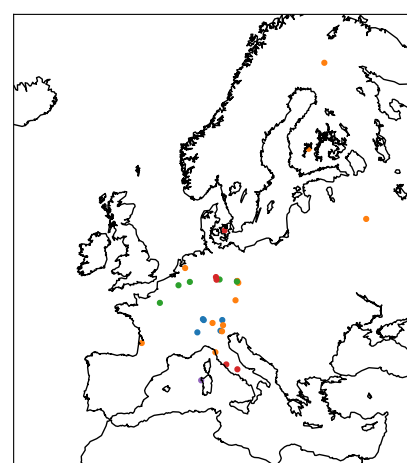
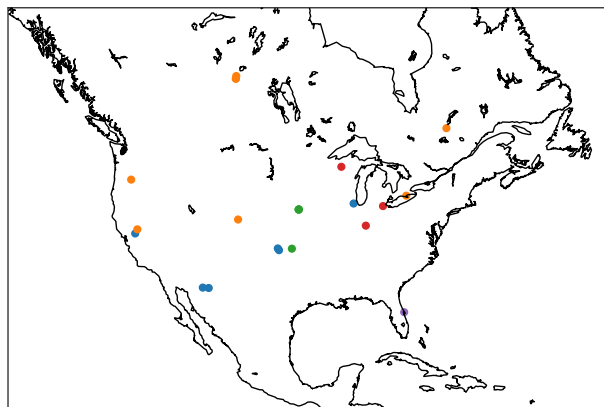
## References

- Franks, P. J., J. A. Berry, D. L. Lombardozzi, and G. B. Bonan (2017), Stomatal function across temporal and spatial scales: Deep-time trends, land-atmosphere coupling and global models, *Plant Physiology*, 174(2), 583–602, doi:10.1104/pp.17.00287.
- Lin, Y.-S., B. E. Medlyn, R. A. Duursma, I. C. Prentice, H. Wang, S. Baig, D. Eamus, V. R. de Dios, P. Mitchell, D. S. Ellsworth, M. O. de Beeck, G. Wallin, J. Uddling, L. Tarvainen, M.-L. Linderson, L. A. Cernusak, J. B. Nippert, T. W. Ocheltree, D. T. Tissue, N. K.

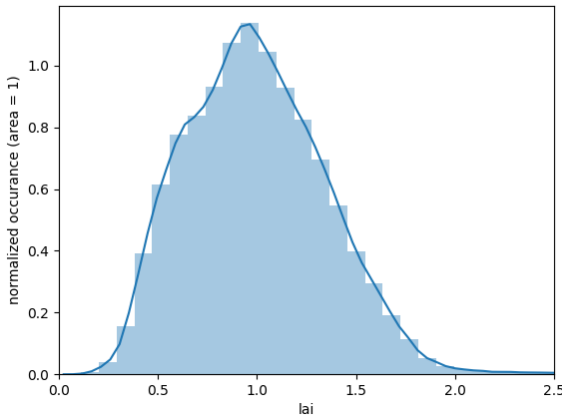
Martin-StPaul, A. Rogers, J. M. Warren, P. D. Angelis, K. Hikosaka, Q. Han, Y. Onoda,  
T. E. Gimeno, C. V. M. Barton, J. Bennie, D. Bonal, A. Bosc, M. LÃºw, C. Macinins-  
Ng, A. Rey, L. Rowland, S. A. Setterfield, S. Tausz-Posch, J. Zaragoza-Castells, M. S. J.  
Broadmeadow, J. E. Drake, M. Freeman, O. Ghannoum, L. B. Hutley, J. W. Kelly,  
K. Kikuzawa, P. Kolari, K. Koyama, J.-M. Limousin, P. Meir, A. C. L. da Costa, T. N.  
Mikkelsen, N. Salinas, W. Sun, and L. Wingate (2015), Optimal stomatal behaviour  
around the world, *Nature Climate Change*, 5(5), 459–464, doi:10.1038/nclimate2550.

MEDLYN, B. E., R. A. DUURSMA, D. EAMUS, D. S. ELLSWORTH, I. C. PRENTICE,  
C. V. M. BARTON, K. Y. CROUS, P. D. ANGELIS, M. FREEMAN, and L. WINGATE  
(2011), Reconciling the optimal and empirical approaches to modelling stomatal conduc-  
tance, *Global Change Biology*, 17(6), 2134–2144, doi:10.1111/j.1365-2486.2010.02375.x.

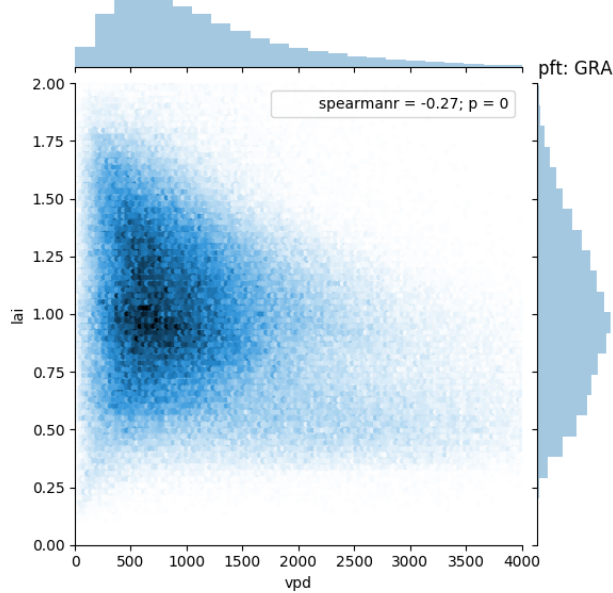
Zhou, S., B. Yu, Y. Huang, and G. Wang (2015), Daily underlying water use efficiency for  
AmeriFlux sites, *Journal of Geophysical Research: Biogeosciences*, 120(5), 887–902, doi:  
10.1002/2015jg002947.



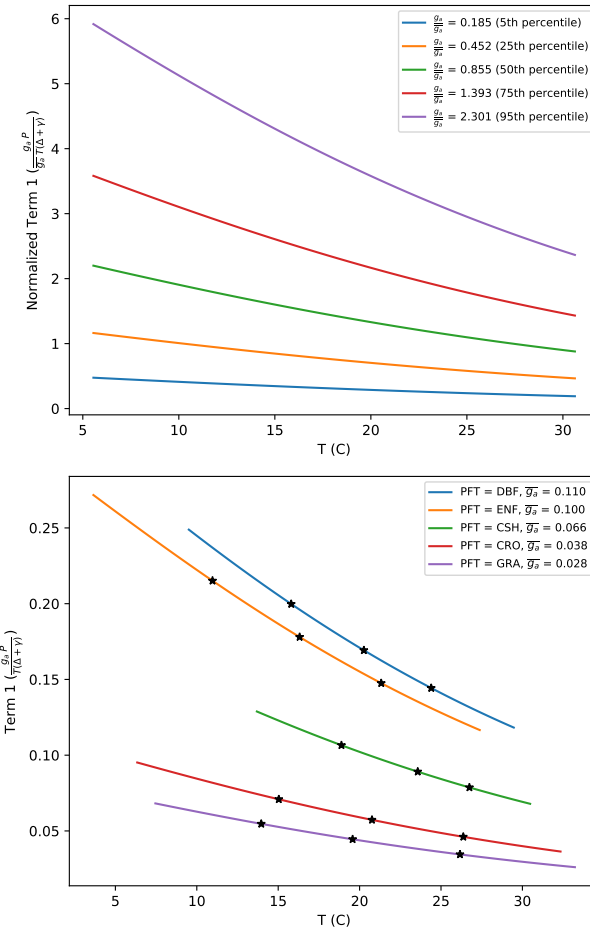
82 **Figure 1.** Plant functional type and location of sites used in analysis. \*\*\*This is just a placeholder for now  
83 and needs to be improved i.e. with lat lon, better placement of continents, etc.)\*\*\*



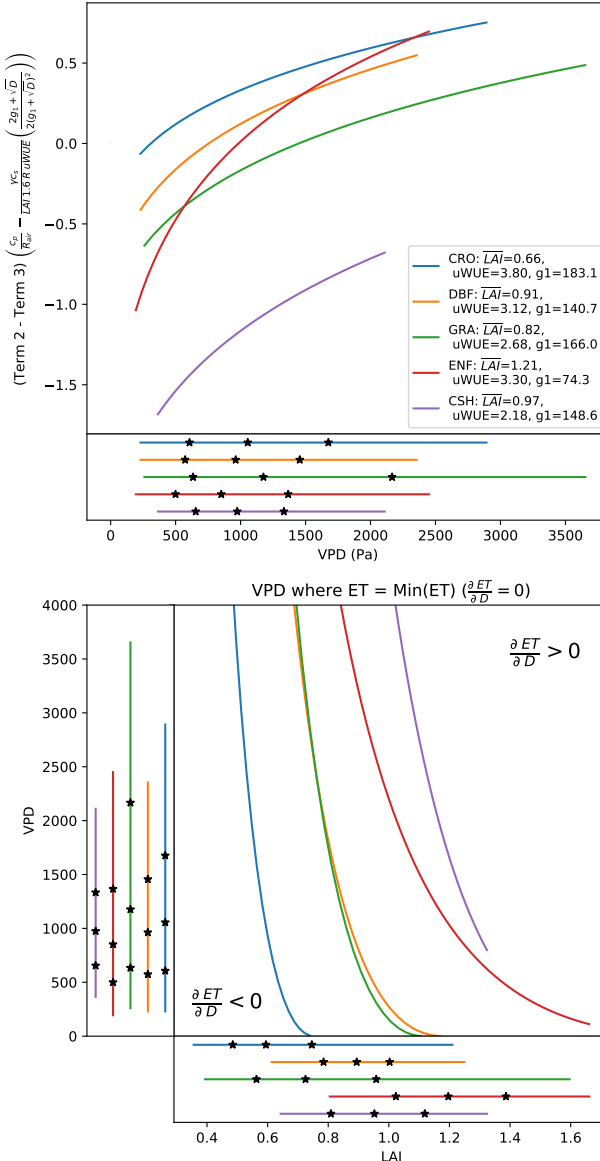
96 **Figure 2.** Histogram of  $\frac{\text{LAI}}{\text{LAI}_{ref}}$  values calculated for each site and time according to Equation 8. The lowest  
97 and highest 5% are removed as outliers, as well as any values below 0. The curve is normalized such that its  
98 area is 1.



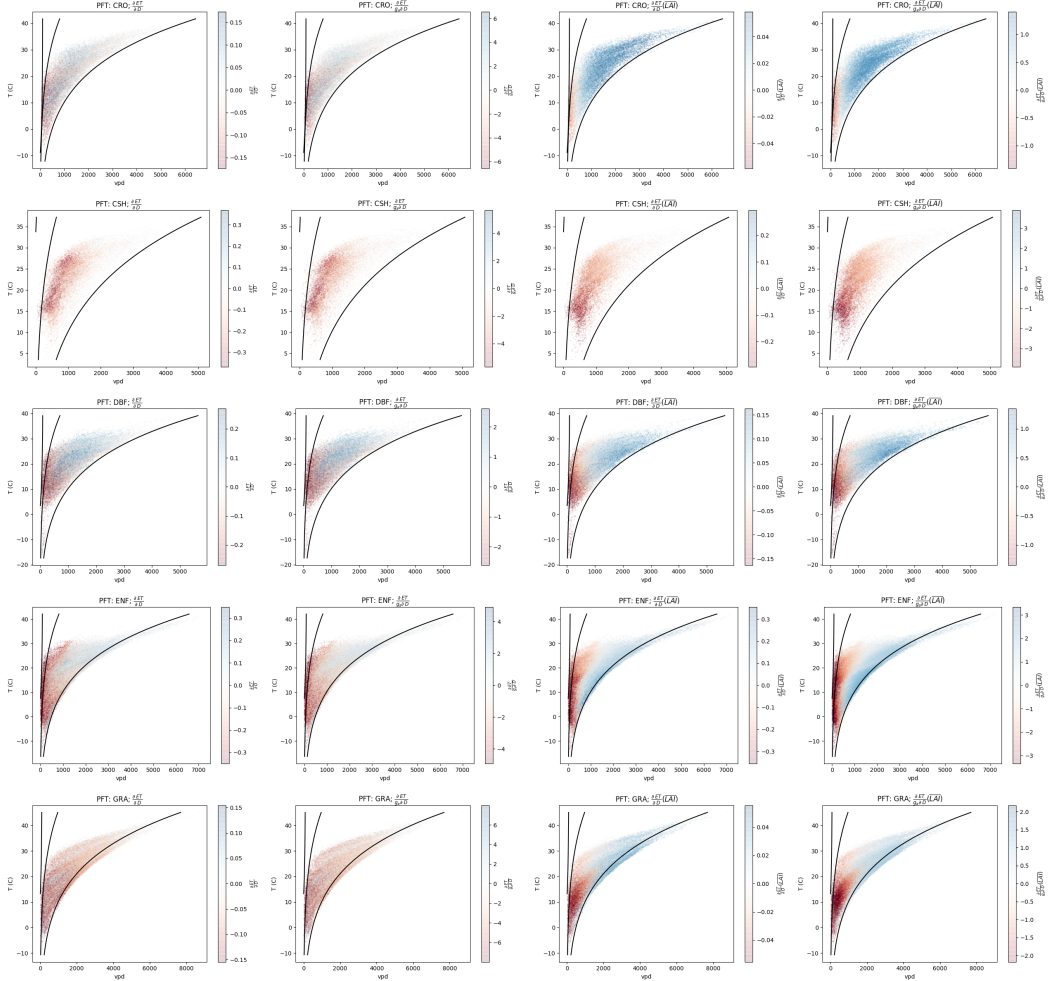
104 **Figure 3.** The joint distribution of  $D$  and  $\frac{\text{LAI}}{\text{LAI}_{ref}}$ .  $\frac{\text{LAI}}{\text{LAI}_{ref}}$  has only a weak dependence on  $D$ . \*\*\*This  
105 plot could probably benefit from a box plot of site specific correlations, because some sites do have stronger  
106 dependence than others. Note also Figs 3 and 2 can probably be combined because this figure shows  $\frac{\text{LAI}}{\text{LAI}_{ref}}$ 's  
107 histogram.\*\*\*



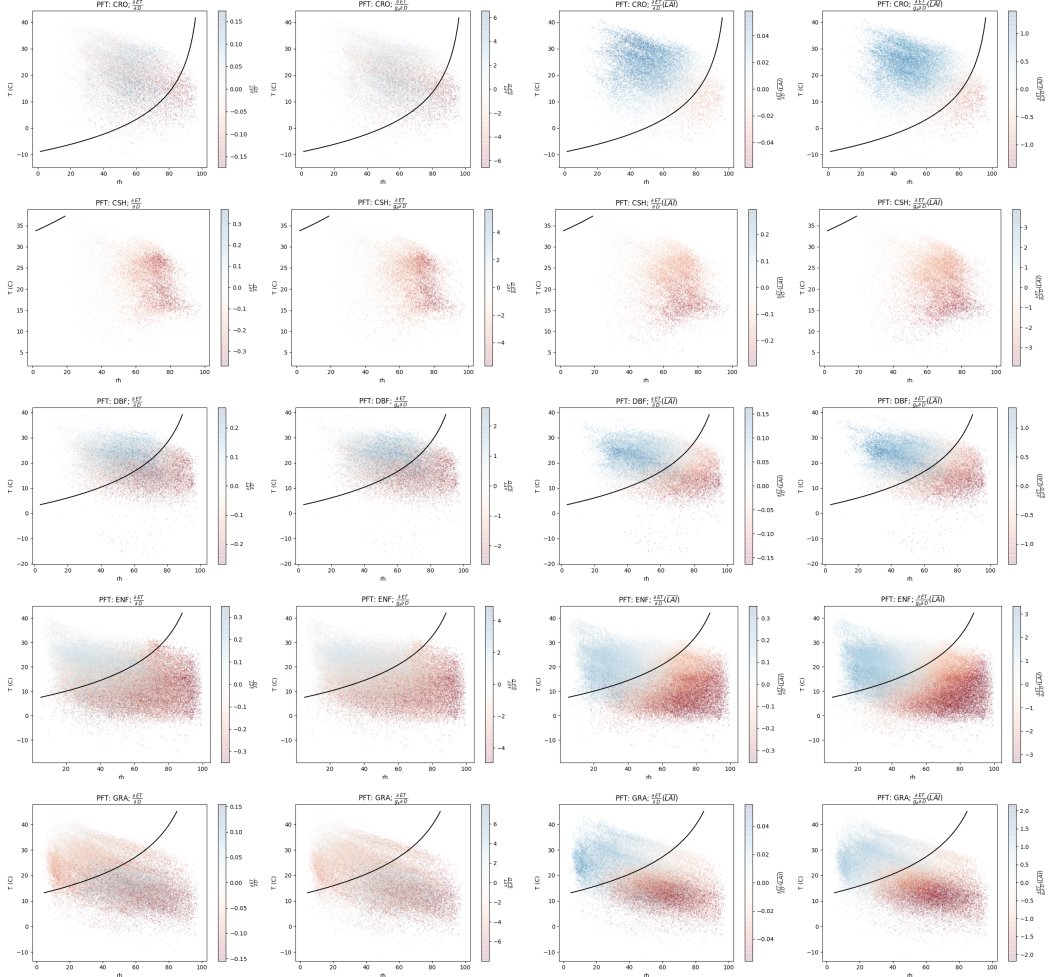
136 **Figure 4.** Primary sources of variability for Term 1. A) Variability within each PFT: Term 1 normalized by  
 137 mean  $g_a$  for each PFT. B) Variability between each PFT: Term 1 evaluated at mean  $g_a$  for each PFT. Tempera-  
 138 ture range is 5-95th percentile for each PFT. Additionally, stars denote the location of the 25th, 50th, and 75th  
 139 percentiles.



147 **Figure 5.** Sources of variability for Term 2 - Term 3. Top: Term 2 - Term 3 as a function of VPD, with  
 148  $\frac{\text{LAI}}{\text{LAI}_{ref}}$  held fixed at PFT averages. The observed range of VPD for each PFT is also shown below the x-axis.  
 149 Line extent corresponds to 5th and 95th percentiles, while stars denote the location of the 25th, 50th, and 75th  
 150 percentiles.  
 151 Bottom: The location of the minima of ET, as a function of VPD and  $\frac{\text{LAI}}{\text{LAI}_{ref}}$ . Lines and stars denote the  
 152 distribution of VPD and  $\frac{\text{LAI}}{\text{LAI}_{ref}}$  next to each axis, following the same percentiles as above.



208 **Figure 6.** Scatter plots of  $\frac{\partial ET}{\partial D}$ . Each row is a different PFT, and each column is a different quantity related  
 209 to  $\frac{\partial ET}{\partial D}$ , as labeled: Column 1 -  $\frac{\partial ET}{\partial D}$ ; Column 2 -  $\frac{\partial ET}{\partial D}$  normalized by  $g_a$ ; Column 3 -  $\frac{\partial ET}{\partial D}$  with  $\frac{LAI}{LAI_{ref}}$   
 210 held fixed at PFT average; and Column 4 -  $\frac{\partial ET}{\partial D}$  normalized by  $g_a$  and with  $\frac{LAI}{LAI_{ref}}$  held fixed. For reference,  
 211 lines corresponding to RH = 20% and RH = 90 % are drawn. Please note differences in the colorbar scale.  
 212 \*\*\*see alternate (or additional) plot below.\*\*\*



220 **Figure 7.** \*\*\*\*alternate Fig 06\*\*\*\* Scatter plots of  $\frac{\partial ET}{\partial D}$ . Each row is a different PFT, and each column  
 221 is a different quantity related to  $\frac{\partial ET}{\partial D}$ , as labeled. If I end up using this, I could also draw on the curve of  
 222  $D_{ETmin}$  with  $\overline{\frac{LAI}{LAI_{ref}}}$ .